Article No. jmbi.1999.2996 available online at http://www.idealibrary.com on IDEAL® J. Mol. Biol. (1999) 291, 801–813

JMB

Domain Organization of Mac-2 Binding Protein and its Oligomerization to Linear and Ring-like Structures

Shirley A. Müller[1], Takako Sasaki[2], Peer Bork[3], Bettina Wolpensinger[1], Therese Schulthess[1], Rupert Timpl[2], Andreas Engel[1] and Jürgen Engel[1]*

[1]*Biozentrum, University of Basel, CH-4056 Basel Switzerland*

[2]*Max-Planck-Institut für Biochemie, D-82152 Martinsried, Germany*

[3]*Max-Delbrück-Center for Molecular Medicine, D-13125 Berlin-Buch and European Molecular Biology Laboratory D-69117 Heidelberg, Germany*

**Corresponding author*

The multidomain Mac-2 binding protein (M2BP) is present in serum and in the extracellular matrix in the form of linear and ring-shaped oligomers, which interact with galectin-3, fibronectin, collagens, integrins and other large glycoproteins. Domain 1 of M2BP (M2BP-1) shows homology with the cysteine-rich SRCR domain of scavanger receptor. Domains 2 and 3 are related to the dimerization domains BTB/POZ and IVR of the *Drosophila* kelch protein. Recombinant M2BP, its N-terminal domain M2BP-1 and a fragment consisting of putative domains 2, 3 and 4 (M2BP-2,3,4) were investigated by scanning transmission electron microscopy, transmission electron microscopy, analytical ultracentrifugation and binding assays. The ring oligomers formed by the intact protein are comprised of approximately 14 nm long segments composed of two 92 kDa M2BP monomers. Although the rings vary in size, decamers predominate. The various linear oligomers also observed are probably ring precursors, dimers predominate. M2BP-1 exhibits a native fold, does not oligomerize and is inactive in cell attachment. M2BP-2,3,4 aggregates to heterogeneous, protein filled ring-like structures as shown by metal shadowed preparations. These aggregates retain the cell-adhesive potential indicating native folding. It is hypothesized that the rings provide an interaction pattern for multivalent interactions of M2BP with target molecules or complexes of ligands.

Keywords: extracellular matrix; assembly; SRCR domain; BTB/POZ+IVR domain; electron microscopy

Introduction

Mac-2 binding protein (M2BP) is a cell-adhesive protein present in restricted localizations of the extracellular matrix and pericellular space of several tissues including testis, thymus, spleen and skeletal muscle (Ullrich *et al.*, 1994; Sasaki *et al.*, 1998). It is also present in extracellular fluids such as serum and milk, is frequently found in the cell medium of cultured cells, for example non-transfected human kidney EBNA-293 cells and has been identified as a tumor-associated antigen (Natali *et al.*, 1982; Iacobelli *et al.*, 1986, 1993; Linsley *et al.*, 1986). It has been suggested that M2BP is involved in the host response to tumors and infections (Ullrich *et al.*, 1994), a notion which is consistent with a recently observed down-modulation of the endotoxin and proinflammatory response in M2BP deficient mice (Trahey & Weissman, 1999). Otherwise the mice showed no phenotype which may provide a clue for other essential functions of the protein.

Mac-2 binding protein received its name from its strong binding to galectin-3 (former name Mac-2) but it also interacts strongly with other extracellular proteins such as collagens IV, V and VI, fibronectin and nidogen (Rosenberg *et al.*, 1991; Koths *et al.*, 1993; Inohara & Raz, 1994; Sasaki *et al.*,

Abbreviations used: FWHM, full width at half maximum mass profile height; M2BP, Mac-2 binding protein; M2BP-1, domain 1 of M2BP; M2BP-2,3,4, M2BP with domain 1 deleted; *n*, number of measurements; PCAP, pancreas cancer associated protein; PIBP, peptidyl prolyl isomerase binding protein; PLZF, BTB/POZ domain of the zinc binding protein; SR, scavenger receptor; SRCR, scavenger receptor Cys-rich domain; STEM, scanning transmission electron microscopy.

E-mail address of the corresponding author: engel@ubaclu.unibas.ch

0022-2836/99/340801–13 $30.00/0

1998). An interaction with cyclophilin C/prolyl *cis-trans* isomerase has been reported for the mouse orthologues of human M2BP (Friedman *et al*., 1993; Chicheportiche & Vasalli, 1994). The protein also mediates cell attachment activity of several cell lines at comparable strength with laminin. This activity is inhibited by an antibody against β1-integrins, suggesting binding of M2BP to this class of receptors.

The molecular mass of a M2BP-monomer is 92 kDa. This value is reduced by 30 % after treatment with *N*-glycosidase F indicating extensive glycosylation. Monomers are only found under strongly denaturing conditions. In physiological buffers M2BP has a high association tendency (Linsley *et al*., 1986; Iacobelli *et al*., 1993; Koths *et al*., 1993) and self-assembly products exhibit average molecular masses between 1000 and 1500 kDa (Sasaki *et al*., 1998). For biochemical and biophysical characterization M2BP was isolated in recombinant form from the culture medium of EBNA-293 kidney cells (Sasaki *et al*., 1998). Inspection of the protein by conventional electron microscopy revealed a large number of ring-like structures with diameters of 30 to 40 nm (Sasaki *et al*., 1998).

In the present work scanning transmission electron microscopy (STEM) of unstained specimens and other techniques were employed to study the mode of the unusual assembly. In addition, the domain organization of M2BP was explored by homology searches and the properties of recombinantly expressed putative domains were compared with those of the parent protein.

Results

Scanning transmission electron microscopy (STEM) of M2BP

Recombinant human M2BP was purified from serum-free culture medium by ammonium sulfate precipitation and column chromatography on Sepharose CL-6B in the presence of protease inhibitors (EDTA, Pefabloc). The protein was adsorbed onto ultra-thin carbon films from 0.2 M ammonium bicarbonate (pH 7.9) and washed with 0.1 M ammonium acetate. After freeze-drying, the unstained particles were visualized by dark field STEM. The low dose images revealed a mixture of rings with variable diameters, and linear oligomers of variable length (FigXure 1). In agreement with previous findings by other electron microscopic techniques (Sasaki *et al*., 1998), many rings were clearly formed from 14.4(±0.4) nm long segments. In addition, a filament of similar length quite often extended towards their interior or a distinct thickening of one or more of the ring segments was observed (arrows). Approximately 2 % of all the rings present exhibited the uniform thickening of all segments. Occasionally two rings appeared to be joined at one point (arrowhead). The smallest number of segments seen to form a ring was four, while up to seven segments could be visually identified. As confirmed by mass analysis (see below), larger rings were also present. The linear aggregates also often appeared to be segmented. However, these could not always be classified according to their length or number of segments since particularly the lower oligomers were not always fully extended. Instead, a classification was made according to their mass determined by the STEM technique (Figure 2).

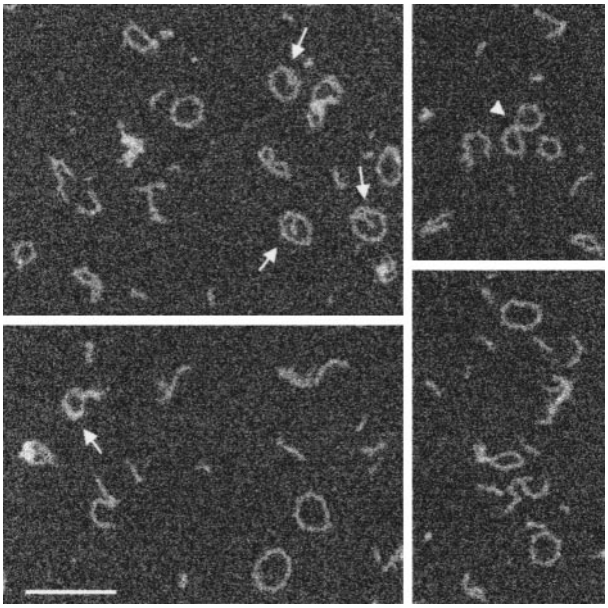

Figure 1. Fields of linear and ring-like unstained M2BP oligomers visualized by scanning transmission electron microscopy. Additional structures or the thickening of ring segments was sometimes observed (arrows). Occasionally two rings appeared to be joined (arrowhead). The bar represents 100 nm.

Molecular masses and distribution of linear oligomers

More than 1000 linear oligomers were selected and measured (see Materials and Methods). The resulting absolute mass values were split into three groups according to the size of the field required for oligomer selection, displayed in histograms and analyzed by Gaussian curve fitting (Figure 2). The distribution from particles with the smallest dimensions, peaked at a mass of 180(±50) kDa, identifying the oligomers as M2BP dimers (approximately 57 % of all linear oligomers). The shoulder in the distribution at 297(±35) kDa would be compatible with the presence of about 18 % trimers. The average particle length of 46 selected dimers that were considered to be fully extended on the carbon film, was 14(±2) nm. The mass values from the two groups of longer oligomers displayed distinct maxima at 363(±76) kDa and 560(±103) kDa, respectively, indicating the presence of approximately 14 % tetramers and 13 %

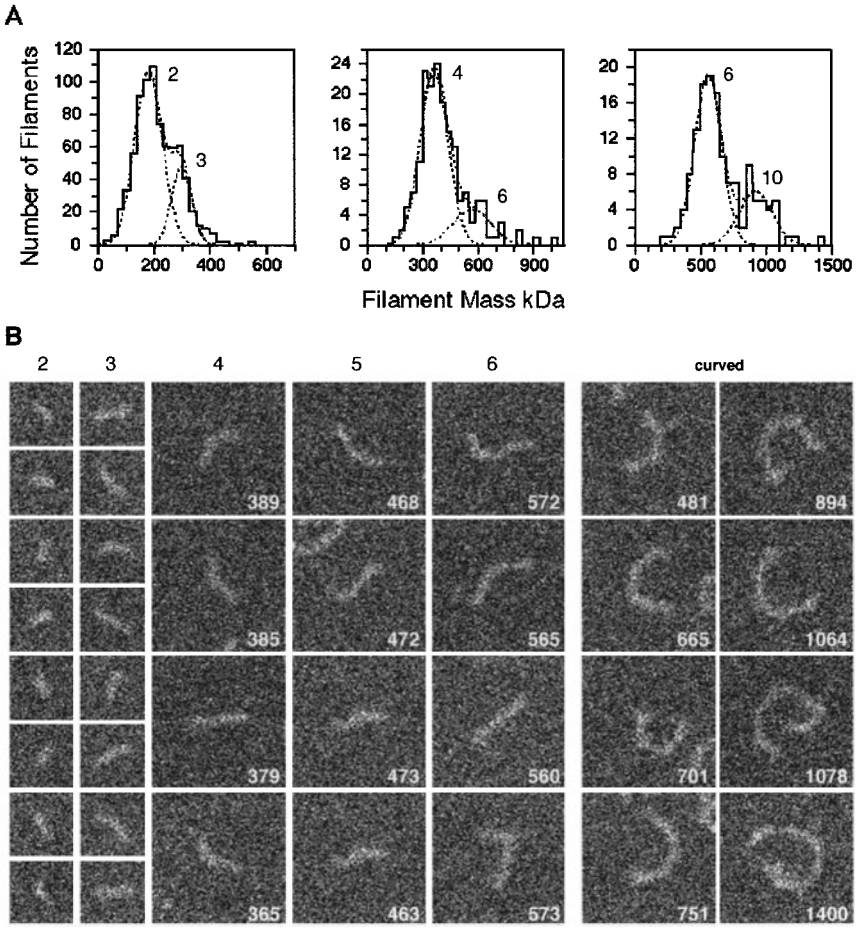

Figure 2. Mass determination of linear oligomers. (a) Histograms of molecular masses. The distributions peak at 180(±50) kDa ($n \approx 570$) and 297(±35) kDa ($n \approx 200$), 363(±76) kDa ($n \approx 150$) and 570(±103) kDa ($n \approx 30$), 560(±103) kDa ($n \approx 140$) and 923(±128) kDa ($n \approx 40$), on the three histograms respectively. The number of M2BP monomers to which these values correspond is indicated. (b) Linear oligomers grouped according to the number of subunits implied by their masses, as given at the top of each column. The molecular masses in kDa are cited in columns 4 to 6. For the first and second columns the values are 170, 188, 184, 181, 190, 188, 179 and 193 kDa and 286, 278, 274, 279, 275, 280, 294 and 274 kDa, respectively (pictures from top to bottom). The two columns on the far left show selected curved oligomers consisting of 4 to 14 monomers. Their molecular masses (in kDa) are cited. The width of the smaller frames represents 35 nm and that of the larger frames 71 nm. In all cases (a) and (b), correction has been made for beam induced mass loss.

hexamers (average of two histograms) in all. Less than 10% of all filaments evaluated were higher oligomers. Species with masses indicating the presence of an odd number of M2BP monomers were also detected; however, with the exception of trimers these were never present in sufficient numbers to yield a distinct peak on the mass histograms. Representative members of the various oligomers are shown in Figure 2(b).

Where possible, the molecular mass-per-length (MPL) ratio was evaluated for the various linear oligomers yielding an average value of 13.1(±2.4) kDa/nm ($n = 149$). This corresponds to a calculated value of 1.99 monomers (92 kDa) per segment of 14 nm length. The average full width at half maximum mass profile height (FWHM) of the evaluated filament stretches was 5.6(±0.8) nm.

Molecular mass of ring structures

As reported in an earlier publication, a large fraction of M2BP oligomers are rings of variable size (Sasaki *et al.*, 1998). A quantitative evaluation of these structures was achieved by STEM mass analysis (Figure 3). Only rings without additional filamentous structures which did not display major variations in segment thickness were considered. Uniform rings for which the number of segments could be clearly distinguished were classified according to size (Figure 3(a)), and their average molecular mass was calculated. The latter was 727(±68) kDa, 925(±86) kDa, 1106(±48) kDa and 1315(±39) kDa for rings with four, five, six and seven segments, respectively. Division of the above values by the molecular mass of monomeric M2BP, showed the number of monomeric subunits present to be consistently twice the number of sides identified. The occurrence of two monomers per segment was confirmed by the independently measured MPL ratio, 13.8(±2.2) kDa/nm ($n = 49$), evaluated from 20(±4) nm long stretches of the ring filaments (Figure 3(b)). The corresponding average filament FWHM was 5.8(±0.7) nm (data not shown). Within the experimental uncertainties, the latter two results exactly match those obtained for the linear oligomers, proving the presence of an identical number of subunits per distance in both structures.

Measurement of the total mass of all the uniform ring structures, including the 2% exhibiting double scattering intensity, yielded a complex histogram displaying a pronounced maximum close to the molecular mass of the five-sided rings (decamers; Figure 3(c)). Further peaks indicated the presence of rings formed from six, seven, eight and ten dimeric segments. A small fraction (5%) of rings

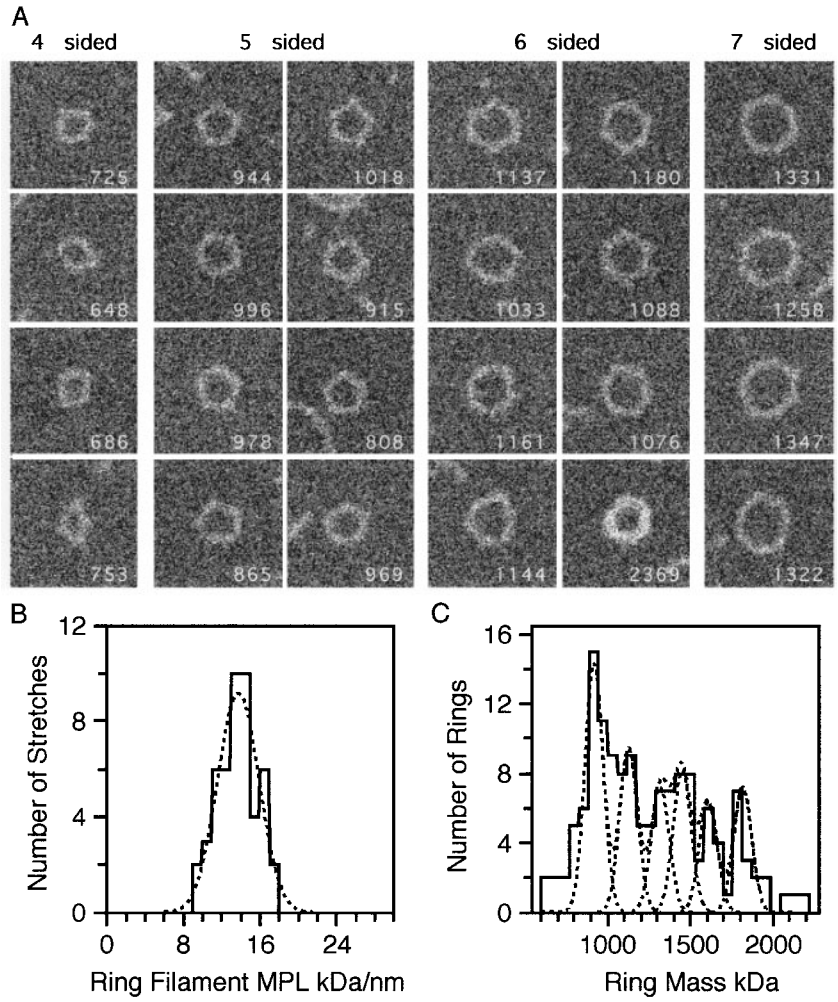

Figure 3. Mass determination of ring-like oligomers. (a) Gallery showing representative rings grouped according to the number of segments visually identified in their circumference. The molecular mass (in kDa) is cited in each frame. Occasionally rings with double scattering intensity were observed (last picture for six sided rings), these were not included on averaging (see the text). The frame width represents 78 nm. (b) Histogram displaying the ring filament MPL ratio 13.8(±2.2) kDa/nm ($n = 49$). (c) Histogram of the uniform ring molecular masses. The six Gaussian peaks fitted fall at 921, 1130, 1319, 1451, 1608 and 1817 kDa and have a standard deviation of 54 kDa. The estimated number of rings giving rise to them is 40, 27, 15, 20, 13 and 14, respectively. The low mass shoulder indicates the presence of a small number of octamers, 710(±53) kDa ($n = 7$). Four higher mass values are not shown. In all cases ((a), (b) and (c)), correction has been made for beam-induced mass loss.

were even heavier. The few mass values arising from four-sided rings showed up as a clear low mass shoulder. Overall, the distribution indicated the presence of approximately 5 % octamers, 28 % decamers, 19 % dodecamers, 10 % 14-mers, 14 % 16-mers, while about 24 % were 18-mers and larger.

Fine structure of linear oligomers and rings

The images recorded at low radiation dose from unstained particles for STEM mass measurement cannot reveal the structural details that are enhanced by rotary shadowing or by negative staining techniques. However, negative staining at neutral pH with phosphotungstate did not provide sufficient resolution and the superior staining with uranyl salts could not be used because of the dissociation of M2BP oligomers at acid pH (Sasaki *et al.*, 1998). Some details of the oligomer architecture could be elucidated using the rotary shadowing technique (Figure 4(a)(d)). However, it should be noted that the accuracy of the dimensions determined is limited by the relatively large correction required to compensate for the effect of metal decoration (see Materials and Methods). The smallest detectable particles were 15-20 nm long and 7(±2) nm wide (Figure 4(a)) and are probably identical to the dimers seen by the STEM mass analysis (Figure 2). In most cases they exhibit a central, only lightly metal decorated region which may indicate a hole, and gives them the appearance of two strands connected at their ends. Larger oligomers are apparently formed by the linear association of such dimers, as indicated by repeating lightly shadowed areas (Figure 4(b) and 4(c)).

Filaments forming the ring-like oligomers did not exhibit the same shadowing pattern. Instead, other structural details were observed at the ring circumference (Figure 4(d)). A slight nodulation of the segments was apparent and sometimes small protrusions were revealed directed into or out of the rings. Similar features were occasionally detectable on STEM images of unstained samples (Figure 3). Metal shadowing also occasionally revealed approximately 14 nm long linear segments extending into or spanning the rings (Figure 4(d)), in agreement with the observations made using negative stain (Sasaki *et al.*,

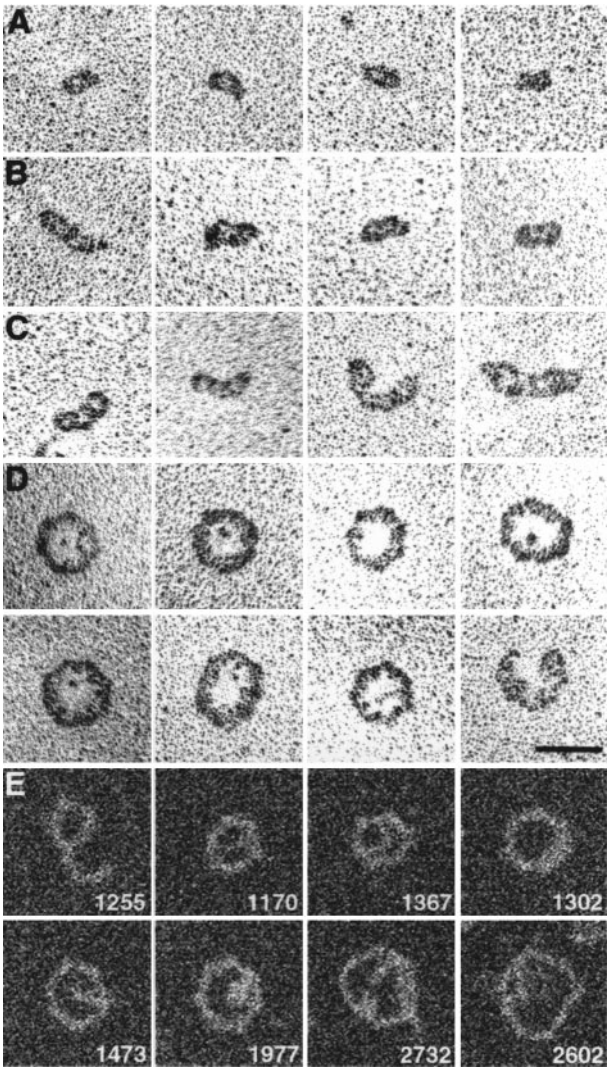

Figure 4. Selected oligomers and ring-like structures visualized by rotary shadowing ((a)-(d)) and STEM (e). (a) Smallest visible oligomers which are interpreted as M2BP dimers. (b) Tetramers probably formed by the linear association of dimers. (c) Larger oligomers formed by the linear association of three dimers. (d) Selected ring structures which show a modularity of the segments and sometimes protrusions at both ends of their ends. (e) Images of rings recorded by STEM from unstained preparations showing the additional features of segment thickening and protruding filaments. The latter sometimes appear to span the ring. Their molecular masses (in kDa) are cited. Correction has been made for beam induced mass loss. The bar represents 50 nm in (a)-(d) while the frame size in (e) is equivalent to 78 nm.

1998) and by STEM (Figures 1(a) and 4(e)). The average width of the ring filaments measured by metal shadowing was 6(±1) nm. From the shadow lengths seen on electron micrographs recorded from samples which had been unidirectionally shadowed with platinum (data not shown), the height of the rings was 7(±2) nm, indicating that the ring filaments are only slightly higher than wide.

Homology searches and sequence analysis

The sequences of human M2BP and two homologous proteins named hamster pancreas cancer associated protein PCAP (70.5 % identity) and mouse peptidyl prolyl isomerase binding protein PIBP (69.8 % identity) are shown in Figure 5. A fourth published sequence of cyclophilin C binding protein (Friedman *et al.*, 1993) turned out to be identical to PIBP (Chicheportiche & Vassali, 1994) after the correction of several sequence errors. (E. Kohfeldt & R. T., unpublished data). PCAB and PIBP are most likely the hamster and mouse orthologues of human M2BP. For cyclophilin C binding protein (=PIBP) this was recently supported by a Southern blot analysis of the mouse genome (Trahey & Weissman, 1999).

Four putative domains can be distinguished in the sequence of M2BP (Figure 5). The sequence region 19 to 133 (domain 1 of M2BP) is homologous to the scavenger receptor Cys-rich (SRCR) domain which is also shared by surface receptors CD5, CD6, complement factor I, and several other proteins (Freeman *et al.*, 1990; Resnik *et al.*, 1994; Pearson, 1996). The crystal structure of this domain of M2BP has been solved (Hohenester *et al.*, 1999).

For the following region in M2BP (127-407) PSI-Blast searches (Altschul *et al.*, 1997) with very restrictive cutoffs (*E*-values $< 10^{-5}$) find a high significance for members of the BTB/POZ + IVR domain family (Figure 6). A *Caenorhabditis elegans* member of this family already matched with a value of 5×10^{-8} in the first search and showed 25 % identity and 41 % similarity with human M2BP. *Drosophila* kelch protein (Robinson & Cooley, 1997), a prominent member of this family matched with a value of 10^{-6} in the second iteration and exhibited 15 % identity and 30 % similarity. The latter protein is an oligomeric ring canal actin organizer which consists of four domains named NTR, BTB/POZ, IVR and KREP. The similarity with M2BP is restricted to the BTB-IVR region, which mediates dimerization of the kelch protein (Robinson & Colley, 1997). Figure 6 also includes the comparison with a BTB/POZ domain of the zinc binding protein PLZF whose crystal structure is known (Ahmad *et al.*, 1998). The boundaries of the BTB and IVR region (domains 2 and 3 in M2BP) are indicated in Figure 5. No convincing similarity with other proteins was detectable for the C-terminal putative domain 4 of M2BP starting at position 451. The sequence of domain 4 is consistent with a globular fold and contains four cysteine residues This domain is linked to domain 3 by a putative link region which is characterized by a high fraction of polar residues and low similarity between the three species variants (Figure 5). The link region contains a plasmin cleavage site at position 441 which was detected by partial sequencing of M2BP fragments after limited plasmin digestion (Sasaki *et al.*, 1998).

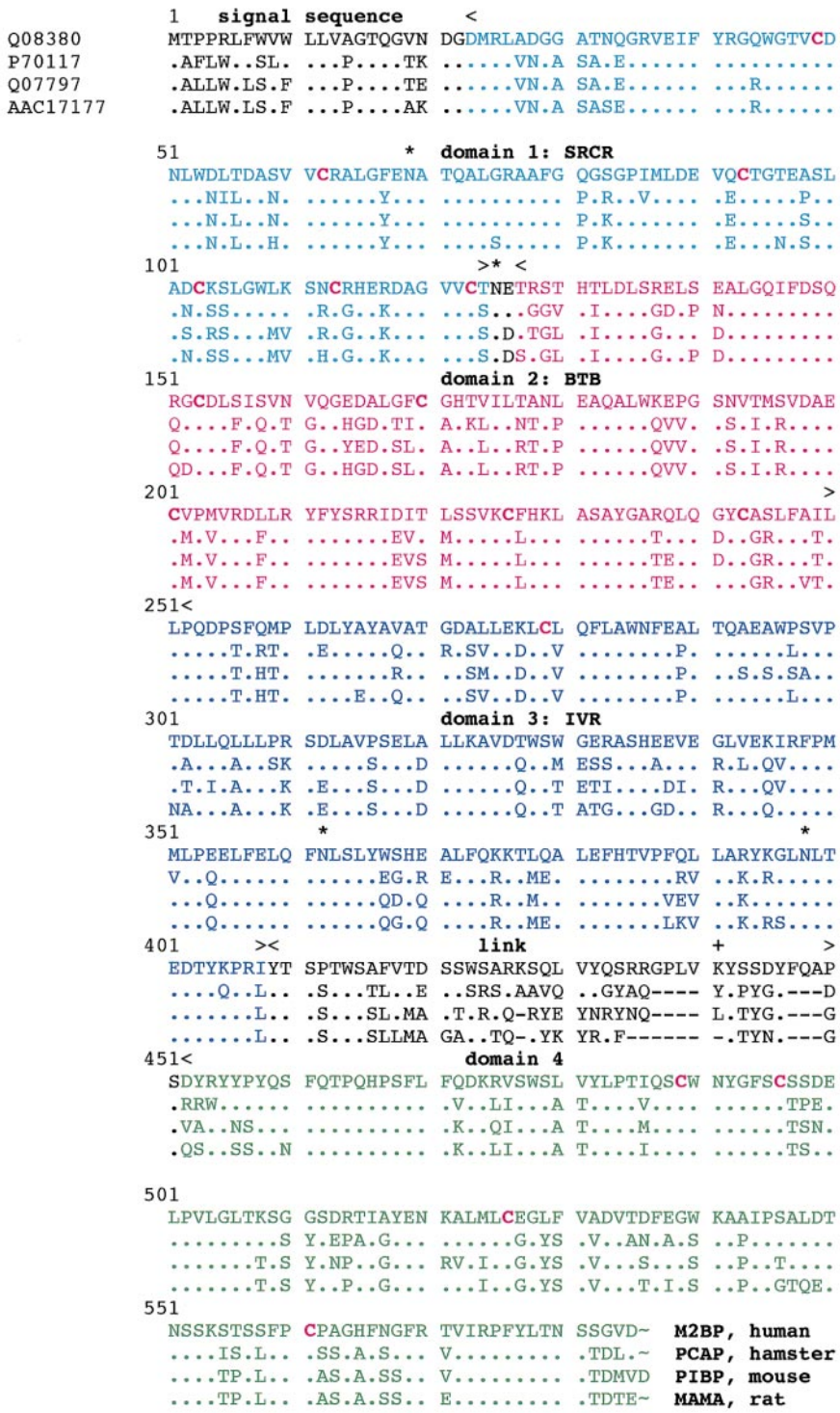

Figure 5. Sequence of human M2BP, hamster pancreas cancer associated protein (PCAP), mouse peptidyl prolyl isomerase binding protein (PIBP) and rat MAMA protein. The signal sequence, domains 1 (SRCR), 2 (BTB/POZ), 3 (IVR), a putative link region and a proposed C-terminal domain 4 are indicated by different colors and >< signs. Residues matching with M2BP are indicated by dots and gaps by dashes. Putative glycosylation sites are marked by an asterisk (*) and a plasmin cleavage site in M2BP by +. Accession numbers refer to SWISSPROT and SPTREMBL databases.

Recombinant production and properties of M2BP domains

Domain 1 (M2BP-1) and the fragment consisting of domains 2, 3 and 4 (M2BP-2,3,4) predicted for M2BP (Figure 5),were recombinantly produced in EBNA-293 kidney cells. Episomal expression vectors were produced by PCR amplification according to domain borders 19-123 for M2BP-1 and 128-585 for M2BP-2,3,4 and joined to a signal

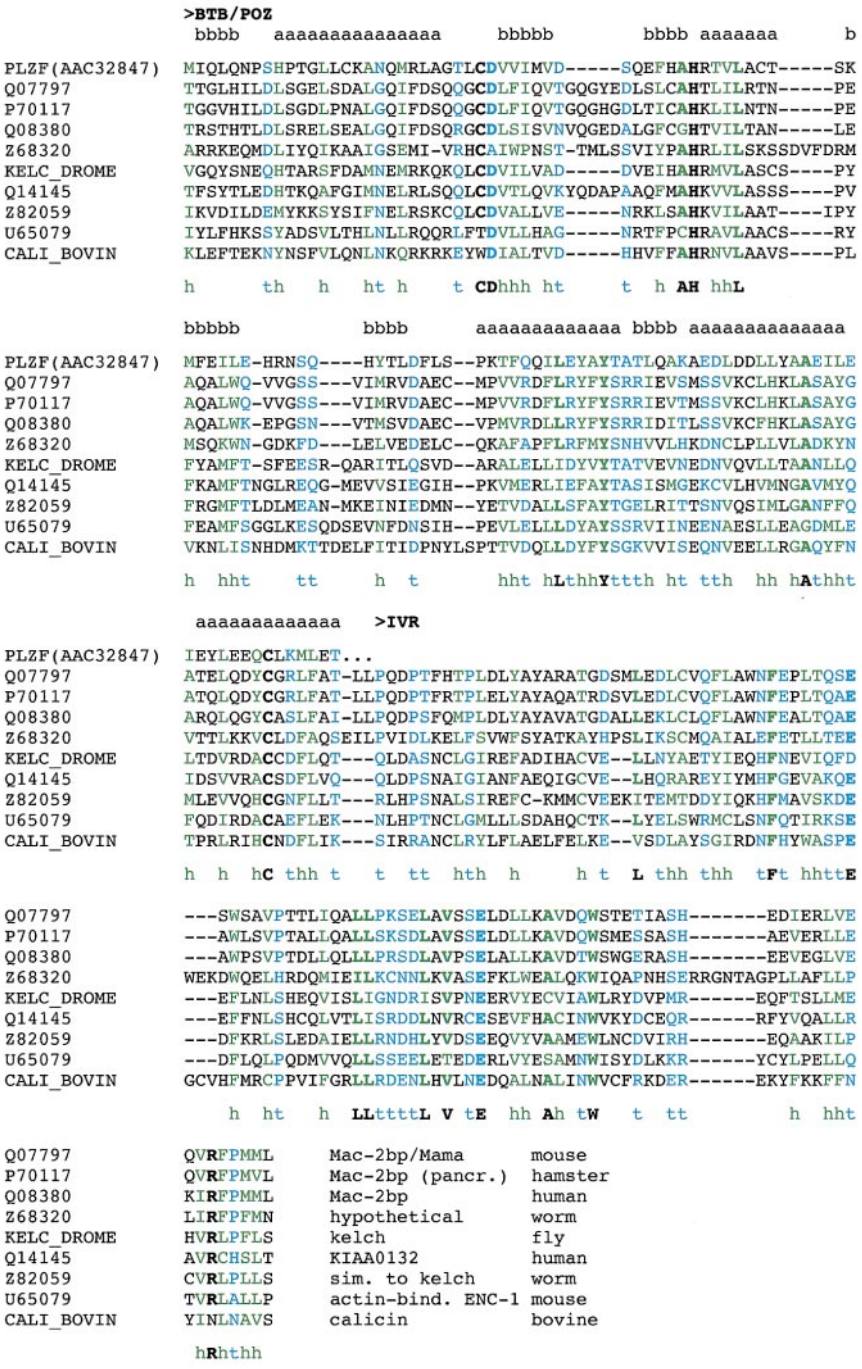

Figure 6. Comparison of the sequence region 127-407 of human M2BP with proteins which contain BTB/POZ domains or pairs of a BTB/POZ and an IVR domain. The junction between the two domains (indicated by >IVR) follows from the crystal structure of the BTB domain in the zinc finger protein PLZF (Ahmad *et al.*, 1998). Residues in α-helices and β-strands in this structure are marked by a und b, respectively. In the lower line residues conserved in at least seven of nine (eight of ten, respectively) sequences are indicated by bold letters and predominantly hydrophobic and polar/turn-like residues by h (green letters in the sequence) and t (blue letters in the sequence). Accession numbers consisting of a letter and five digits refer to the EMBL database and the others to SWISSPROT library identifiers.

peptide sequence (Kohfeldt *et al.*, 1997), which facilitated detection and purification of the recombinant proteins from serum-free culture medium.

Recombinant M2BP-1, which exhibits a prominent homology to the SRCR domain, was readily purified in the form of two fragments (about 27 and 17 kDa) with different electrophoretic mobilities (see Figure 7, lanes 1 and 2). These both started with the same single N-terminal sequence APLAVDG, the APLA being derived from the foreign BM-40 signal peptide cleavage region (Kohlfeldt *et al.*, 1997). Mass spectrometry demon-

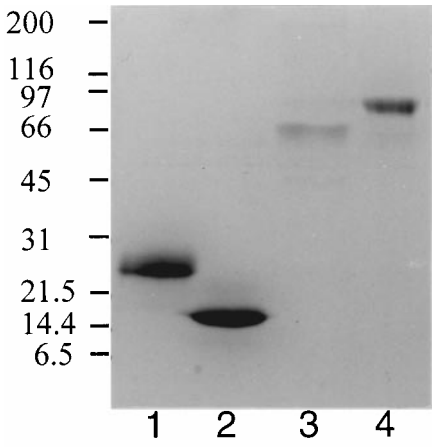

Figure 7. SDS-gel electrophoresis of purified recombinant fragments of M2BP. Samples analyzed were M2BP-1, slower migrating form (lane 1), faster migrating form (lane 2), M2BP-2,3,4 (lane 3) and recombinant M2BP (lane 4), which ran at a mass of about 95 kDa. The latter band was also present in trace amounts in lane 3 as demonstrated by immunoblotting (data not shown). The run was calibrated with marker proteins as indicated in kDa (left margin).

strated two approximately equal signals of 18,273 and 18,559 Da for the slower migrating form and about equal peaks with 14,750 and 14,953 Da for the faster migrating form clearly exceeding the mass calculated from the sequence (12,687 Da). This indicates a variable degree of *N*-glycosylation as also demonstrated by ten residues of glucosamine in the slower migrating form *versus* 3.5 residues in the faster migrating form.

The slower migrating form of M2BP-1 sedimented as a single sharp profile at a sedimentation constant of 2.1 S. Equilibrium experiments yielded a molecular mass of 20(±2) kDa. A frictional ratio $f/f_o = 1.04$ was calculated from the sedimentation constant and the molecular mass determined by mass spectroscopy, indicating an almost perfect spherical shape. Electron micrographs recorded from metal shadowed preparations, also suggested a spherical shape (data not shown) in agreement with X-ray crystallography (Hohenester *et al.*, 1999). In view of the high oligomerization potential of M2BP it is important to note that M2BP-1 did not associate according to ultracentrifugal and electron microscopic evidence.

Recombinant M2BP-2,3,4 was more difficult to purify and required higher NaCl concentrations in the initial steps to assure good solubility (see Materials and Methods). It was finally obtained as a 70 kDa electrophoretic band with only small contamination by endogenous M2BP (Figure 7, lane 3) and showed a single N-terminal APLATRST sequence, the APLA being derived from the expression vector (Kohlfeldt *et al.*, 1997). In 0.2 M ammonium bicarbonate (pH 7.4) strong aggregation was demonstrated by analytical ultracentrifugation. The sedimentation profile showed three steps of about equal size with sedimentation constants of about 20 S, 45 S and 63 S. The average molecular mass was between 6000 and 7000 kDa, indicating about 80 monomers of M2BP-2,3,4 per aggregate on average. The circular dichroism spectra (not shown) closely resembled the published spectra of intact M2BP (Sasaki *et al.*, 1998) showing the fragment to have its native structure. Electron microscopy after rotary shadowing revealed clusters of rings, which were filled with mass in contrast to the ring-like structures formed by intact M2BP (Figure 8). The small number of unfilled rings seen in Figure 8 may originate from contaminating endogenous M2BP which may also be responsible for the 20 S-fraction in the sedimentation profile.

Recombinant M2BP has previously been shown to mediate strong cell adhesion through β1 integrins (Sasaki *et al.*, 1998). This activity was lost after reduction and alkylation of disulfide bonds under denaturing conditions. When tested, M2BP-2,3,4 showed the same cell-adhesive activity as M2BP for Rugli glioma cells while both forms of M2BP-1 were inactive (Figure 9). The same results were also obtained with rat RN22 Schwannoma cells and human HBL-100 cells (data not shown). Similar binding to the extracellular matrix proteins fibronectin, nidogen-1, collagen IV and to galectin-3 were observed for the fragment M2BP-2,3,4 and the parent M2BP (Figure 10). In identical assays with both forms of domain M2BP-1 no interaction was observed (data not shown).

Discussion

Under native conditions M2BP is not found in its monomeric state of 92 kDa but forms oligomers with defined structures. Ring-like structures are prominent self-assembly products of M2BP expressed by EBNA-293 human kidney cells. The endogenously produced rings and the rings formed by the recombinantly expressed material look the same under electron microscopy and the high association tendency was also demonstrated for M2BP from different sources (Sasaki *et al.*, 1998). The rings are of variable size and according to STEM mass measurements are formed from an even number of M2BP monomers. Decamers predominate for the rings while dimers are the predominant linear species. Both the linear oligomers and the rings are segmented at intervals of about 14 nm, which resembles the length of a dimer. Linear oligomers are apparently the precursors of rings. Larger linear structures appear to be formed by a linear association of dimers. Very large linear species exhibit a clear curvature and a tendency for ring formation. Finally, in the rings the bending angle between segments is fixed to 72° for five segments (decamers) and to 60° for six segments (dodecamers). A schematic model is shown in Figure 11.

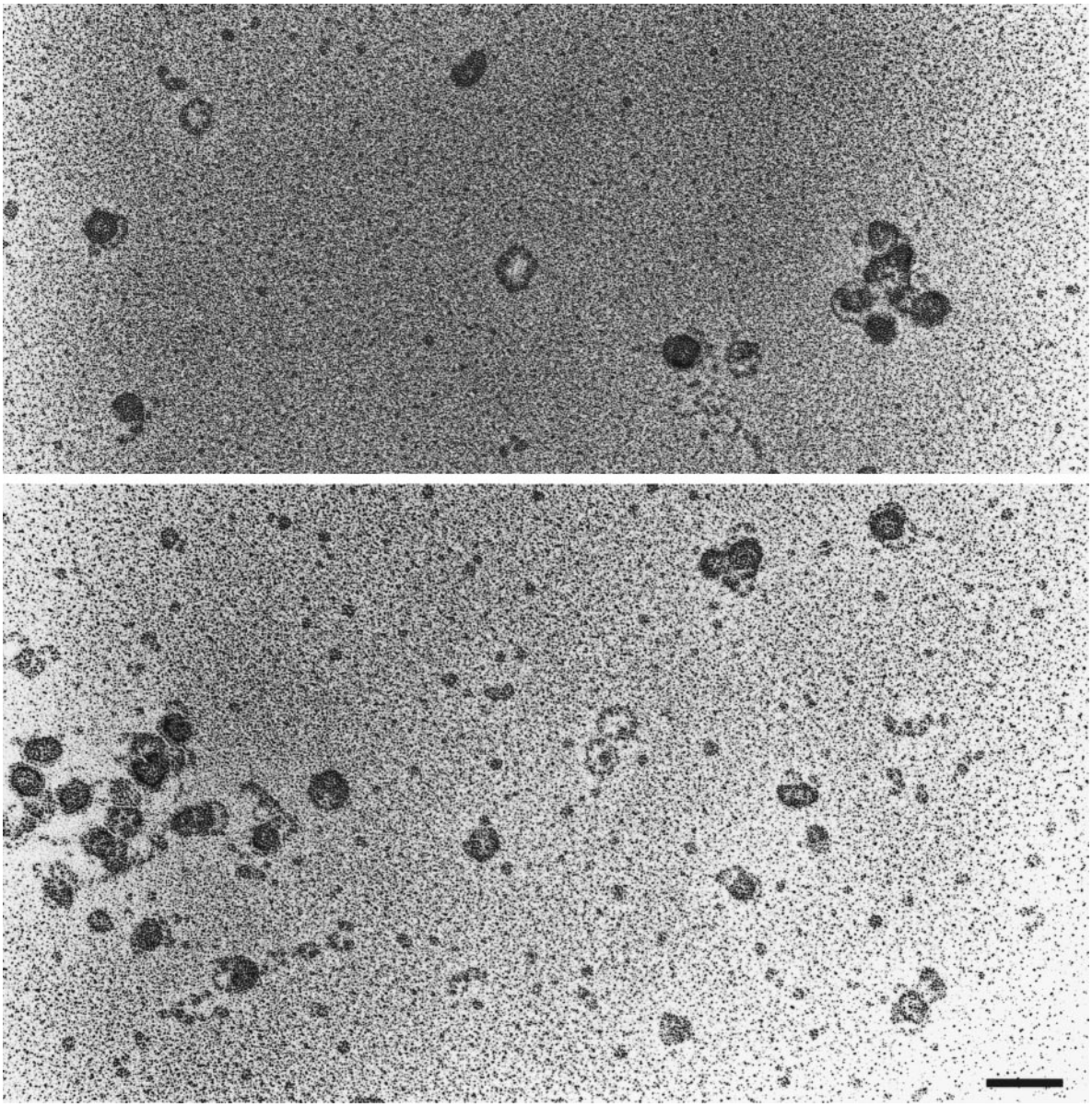

Figure 8. Visualization of the recombinant fragment M2BP-2,3,4 by electron microscopy after rotary shadowing. Abundant clusters of filled rings are interpreted as highly aggregated M2BP-2,3,4 fragments, whereas the minor fraction of open rings may arise from the small impurity of endogenous M2BP. The bar represents 100 nm.

An essential feature of the model and a clear result of mass determinations by STEM is the presence of two monomers per ring segment. All mass data for the ring structures are in clear support of this interpretation. Only a very small fraction of all linear oligomers exhibited masses compatible with an uneven number of monomers. With the exception of trimers, their numbers were never sufficient to yield a defined mass peak on the histograms (Figure 2(a)). Trimers may occur as transient intermediates in the assembly process but in view of its small size, the trimer peak may also originate from impurities. Monomers are apparently only present under strongly denaturing conditions and structure formation requires dimerization (Sasaki *et al.*, 1998).

The observation of obligatory dimer formation by M2BP is in complete agreement with the strong dimerization tendency of many other proteins containing BTB/POZ domains (reviewed by Aravind & Koonin, 1999). A well studied example is the *Drosophila* kelch protein whose dimerization during actin ring canal formation is mediated by a BTB/POZ domain with an IVR domain as its neighbor (Robinson & Cooley, 1997). The crystal structure of the BTB/POZ domain from the zinc finger protein PLZF (Ahmad *et al.*, 1998) revealed a dimer stabilized by an extensive hydrophobic interface. In agreement with this structural evidence, unfolding studies showed that structure formation required dimerization (Li *et al.*, 1997) and the BTB pair was, therefore, called an obliga-

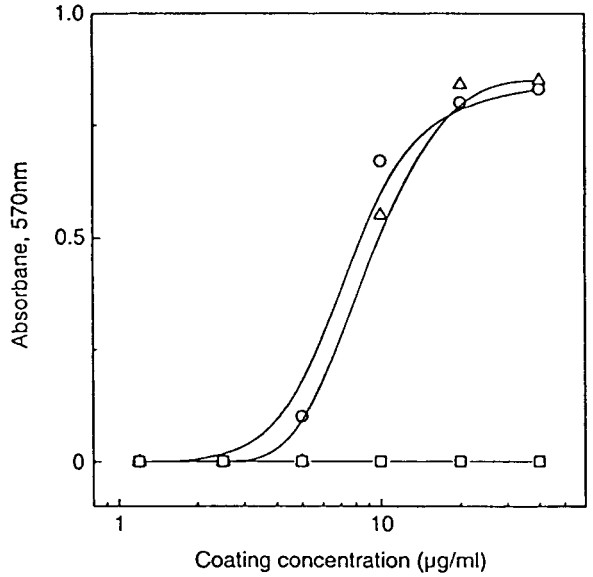

Figure 9. Cell-adhesion profiles of Rugli rat glioma cells for M2BP and its recombinant fragments. Wells were coated with different concentrations of recombinant M2BP (○) and its domain M2BP-1, slower migrating form (□) and fragment M2BP-2,3,4 (△). Adherent cells were measured by a colorimetric assay (Aumailley *et al.*, 1989).

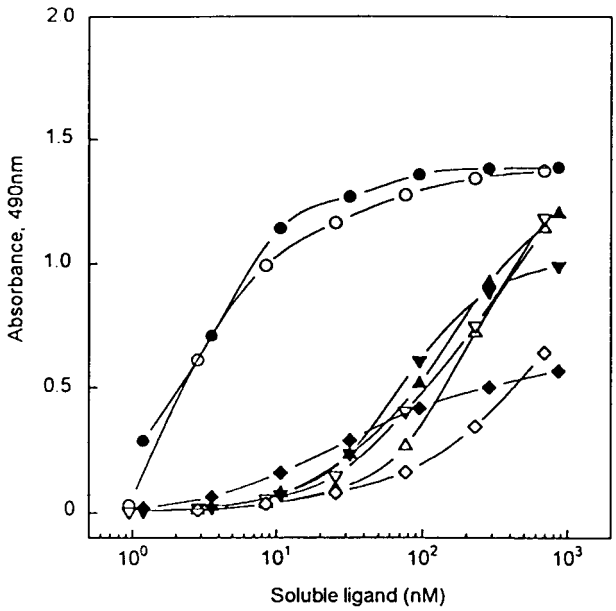

Figure 10. Binding of soluble M2BP and fragment M2BP-2,3,4 to immobilized extracellular matrix ligands in solid-phase assays. Binding to galectin-3 (○), fibronectin (△), nidogen-1 (▽) and collagen IV (◇) to M2BP (open symbols) and M2BP-2,3,4 (filled symbols). The concentrations of the soluble ligands are expressed as monomers.

tory dimer. Because of this prominent property it is suggested that the BTB/POZ domain is responsible for the lateral association of M2BP (Figure 11). According to structural evidence, the BTB/POZ domain forms an intertwisted dimer with the N-terminus of one of its subunits close to the C terminus of the other (Ahmad *et al.*, 1998). However, the two POZ units in the PLZF dimer are arranged in a parallel orientation at their interface. To account for this both domains 2 have been drawn in a parallel arrangement with domains 1 and 3 emerging from the same end of each. There are additional arguments, which favor a parallel alignment of peptide chains in the M2BP-dimer. An antiparallel arrangement would either lead to interactions between different domains within the dimer or to a longer length than observed. It would also produce identical ends.

It is interesting to note that the BTB/POZ domain in M2BP is the first domain of this type clearly defined to be in an extracellular protein. According to Aravind & Koonin (1999) the BTB/POZ domain is either located in the cytosol or its position is undefined in the 81 listed proteins. The Cys residues in the zinc finger binding protein are not connected by disulfide bonds (Ahmad *et al.*, 1998). However, disulfide formation is possible between these and additional cysteine residues in the extracellular M2BP domain and a linkage to the single cysteine in the IVR domain is also possible (Figures 5 and 6).

Fragment M2BP−2,3,4 which starts with the dimerizing BTB/POZ domain also forms rings, but its association is less specific and the rings were found to be filled with protein (Figure 8). Although segments sometimes protruded into the interior of rings formed by unmodified M2BP these were never entirely filled (Figure 4). Apparently the specificity of ring closure is enhanced by the presence of domain 1, which by itself does not exhibit an aggregation tendency. The localization of the sites of interactions leading to ring formation remains to be elucidated. Hypothetically it is assumed that domains 2 and 4 are interacting (Figure 11). It is unlikely that rings of M2BP are precursors of tubes because of the low fraction (>2 %) of rings with twice the molecular mass of single rings and the absence of species with more than two superimposed rings.

The N-terminal domain of M2BP-1 is homologous to the cysteine-rich scavenger receptor (SR) domains of scavenger receptor, the speract cross-linking protein from sea urchin sperm, and the surface receptors CD5 and CD6 (see Hohenester *et al.*, 1999). Its circular dichroism spectra, melting profile, hydrodynamic properties and electron microscopically observed shape are in agreement with the much more detailed information obtained from the recent crystal structure (Hohenester *et al.*, 1999). As already mentioned it has a regulatory function in assembly, and together with the other

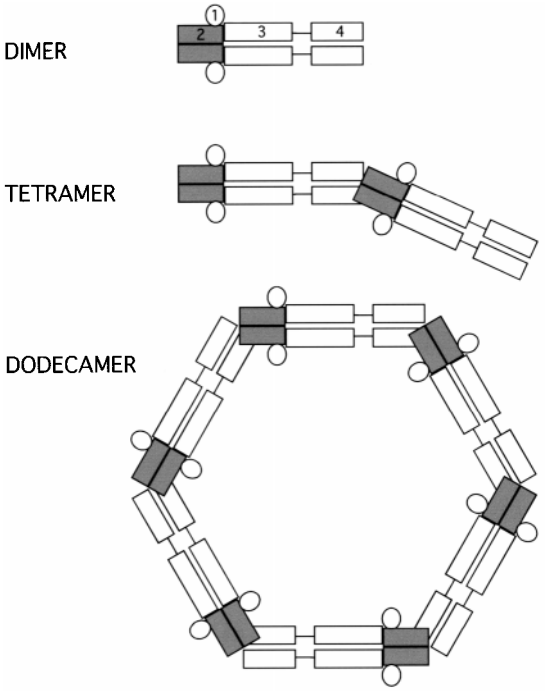

Figure 11. Schematic model of the oligomerization of M2BP. The smallest stable units are dimers which are formed by the interactions between POZ/BTB domains 2 (gray, also see numbers in the upper subunit of the dimer). The SRCR domain 1 does not directly participate in oligomerization and is bound to the POZ/BTB domain at the same end as domain 3. Dimers interact end-to-end, probably *via* domains 2 and 4, to form linear structures with a bending angle at the interface (a tetramer is shown as an example). As oligomerisation increases, a length is reached at which the ends of a linear oligomer can interact to form a ring (a dodecamer is shown as an example).

domains it may mediate the interaction with binding partners of M2BP.

Several functions have been assigned to M2BP. Because of its SRCR domain and occurrence in serum, milk and other secretions it has been speculated that M2BP might be involved in host defence, similar to the scavenger receptor and related proteins (Koths *et al.*, 1993). Cyclophilin C (prolyl *cis-trans* isomerase) binding has been reported and discussed as a possible function of a mouse orthologue of M2BP (Friedman *et al.*, 1993; Chicheportiche & Vasalli, 1994). Our own unpublished work has demonstrated no binding of cyclophilins A and B to M2BP. Gene-targeted M2BP-deficient mice appeared to be healthy but were found to be more sensitive to the lethal effects of endotoxin (Trahey & Weissman, 1999). Other functional implications are based on its binding of galectin-3 (Koths *et al.*, 1993; Inohara & Raz, 1994; Rosenberg *et al.*, 1991). Galectin-3 was found to interact with the extracellular matrix protein laminin (Sato & Hughes, 1992). It was suggested that M2BP may promote cell-cell contacts (Inohara *et al.*, 1996), or regulate cell adhesion (Ochieng *et al.*, 1998) through interactions with galectin-3. However, direct binding of M2BP to extracellular matrix proteins and to their integrin receptors may also be involved in these processes (Sasaki *et al.*, 1998). The exact sites of interactions with ligands have to be elucidated by future work with individual recombinant fragments 2, 3 and 4. At present it is only known that the adhesion function as well as binding to galectin-3, fibronectin, nidogen-1 and collagen IV are localized in a combination of the three domains.

For all suggested functions, the multivalency of M2BP provided by its assembly to ring-like structures may be of decisive importance for the linkage of different components and for an increase in binding activity. Multivalency is certainly important for the strong interaction with the also multivalent galectin-3 (Woo *et al.*, 1991; Yang *et al.*, 1998; Seetharaman *et al.*, 1998). In addition to providing the frame for multivalent interactions, the spatial arrangement of domains in M2BP rings may be of additional functional importance. The rings may be designed to enclose a target molecule or a complex of several molecules. Segments facing into the ring and repeating at a distance of approximately 14 nm may provide an interaction pattern. A third and more trivial reason for self-assembly of M2BP is the need of osmotic pressure reduction for a protein which occurs at relatively high concentrations in extracellular fluids.

Ongoing work is focused on gaining a more detailed definition of the mechanism by which M2BP interacts with its ligands. This may also lead to a deeper understanding of the functional advantage of its ring-like structure.

Materials and Methods

Preparation and characterization of recombinant M2BP fragments

Episomal expression vectors and the recombinant fragment M2BP-1 (Hohenester *et al.*, 1999) corresponding to the scavenger receptor cysteine-rich domain-1 were prepared as described. A similar expression vector for the predicted domain M2BP-2,3,4 was obtained by PCR amplification of a human cDNA (Ullrich *et al.*, 1994) using appropriate oligonucleotide primers corresponding to the domain borders 128 and 585. The correctness of the sequences was verified by dye terminator cycle sequencing. They were inserted into the pCEP-Pu expression vector in frame to the BM-40 signal peptide and used for the episomal transfection of human EBNA-293 cells (Kohfeldt *et al.*, 1997). Transcription into mRNA was analyzed by Northern blots and secretion of proteins into serum-free culture medium was determined by SDS-gel electrophoresis following standard procedures. For the isolation of fragment M2BP-2,3,4, 0.5 litre of serum-free medium was dialyzed against 20 mM Tris-HCl (pH 7.4), 0.5 M NaCl and passed over a column (1 cm × 6 cm) of wheat germ lectin-agarose (Pharmacia) in the same buffer. Bound proteins were eluted with 0.5 M *N*-acetylglucosamine, dialyzed against 20 mM Tris-HCl (pH 8.0), 0.3 M NaCl and passed over Mono Q

HR5/5 equilibrated in the same buffer (Pharmacia). Proteins were eluted with a linear 0.3-0.6 M NaCl gradient and further purified on Superose 6 HR16/50 (Pharmacia), which was equilibrated with 0.2 M ammonium acetate (pH 6.8). Analytical methods and solid-phase binding and cell-adhesion assays followed previously used procedures (Sasaki *et al*., 1998).

Transmission electron microscopy

Electron microscopy by the rotary shadowing technique was performed as described (Engel, 1994). Protein (25-50 μg/ml) in 0.2 M ammonium bicarbonate (pH 7.9) was mixed with an equal volume of glycerol and sprayed onto freshly cleaved mica discs. These were dried in high vacuum, rotary shadowed with platinum/carbon at an angle of 9° and replicated. For evaluation of particle heights shadowing was performed at a fixed angle of 9° and the height was calculated from the shadow length by multiplication with the tangents of 9°. Dimensions were averaged from more than 20 measurements and corrected by subtraction of 3 nm to account for the increase of particle size by decoration with metal crystallites (Engel, 1994).

Scanning transmission electron microscopy (STEM)

The preparation of M2BP complexes (25-50 μg/ml) in 0.2 M ammonium bicarbonate (pH 7.9) was diluted 25 times with 0.2 M ammonium acetate solution and immediately adsorbed to freshly glow discharged thin carbon films. The latter were supported by thick perforated carbon layers (Fukami & Adachi, 1965) on gold-coated copper microscopy grids. The specimens were subsequently washed on four drops of 0.1 M ammonium acetate and freeze-dried at −80 °C overnight in the microscope. Both the grids and the buffer solutions were prepared using quartz bi-distilled water.

A Vacuum Generators HB-5 scanning transmission electron microscope controlled by a modular computer system (Tietz Video and Image Processing Systems GmbH, D-8035 Gauting) was employed for the measurements. Elastic dark field images of the unstained complexes were recorded at 80 kV acceleration voltage and a nominal magnification of 200,000× using electron doses of 346(±14) electrons/nm^2. The digital images were evaluated using the specialized program package, IMPSYS, described by Müller *et al*. (1992). In the initial step, the various species were selected in boxes of various size, thus minimising the effect of fluctuations in the carbon support film scattering. The resulting mass data sets were examined individually. Correction for beam-induced mass loss was made assuming the behaviour of fd-phage (Müller *et al*., 1992) for both the filament and ring structures observed. This necessitated multiplication of the measured mass and MPL ratios by the factor 1.027. In the final step, the corrected mass data were pooled as necessary, displayed in histograms and described by series of Gaussian curves. The results presented are the absolute values.

Molecular mass determinations and circular dichroism

For analytical ultracentrifugation, an Optima XL-A (Beckman Instruments, Fullerston, USA) with an AnS rotor and 12 mm filled Epon cells was employed. Sedimentation constants were evaluated from sedimentation velocity experiments at rotor speeds of 44,000 and 52,000 r.p.m. and corrected to standard conditions (water at 20 °C). Molecular masses were determined from sedimentation equilibrium experiments at 26,000 r.p.m. (domain M2BP-1) and 2400 r.p.m. (fragment M2BP-2,3,4). Measurements were performed at 18 °C in 50 mM Tris-HCl buffer (pH 7.4) containing 0.5 M NaCl and for fragment M2BP-2,3,4 in 0.2 M ammonium bicabonate (pH 7.4). Data evaluation was by standard methods assuming partial specific volumes of 0.680 ml/g for domain M2BP-1 and 0.697 ml/g for fragment M2BP-2,3,4. These are the calculated values for proteins with 45% and 35% weight glycosylation, respectively (Ralston, 1993).

Electrospray ionization mass spectroscopy was performed by our peptide facilities following established procedures.

Circular dichroism spectra were recorded on a Cary 61 spectropolarimeter (Varian, Zug, Switzerland) using a thermostatted cell of 1 mm path length (Hellma, Müllheim, Germany). For the thermal melting profile the temperature was raised at a rate of one degree per minute by means of an automatic programmer. Measurements were performed in the buffers used for analytical ultracentrifugation, and molar ellipticitiy (in deg. cm^2/dmol) was calculated with a mean molecular mass of 110 kDa (Stock *et al*., 1996).

Acknowledgments

This work was supported by the Swiss National Science Foundation to J.E. (grant number 31-49281.96) and A.E. (grant number 31-42435.94), by the Maurice E. Müller Foundation and by an EC grant (Bio4-CT96-0537) to R.T. We are grateful for the expert technical assistance of Vera van Delden, Mischa Reiter and Ariel Lustig, and to Dr Karlheinz Mann for sequence analysis.

References

Ahmad, F. K., Engel, C. K. & Prive, G. G. (1998). Crystal structure of the BTB domain from *PLZF*. *Proc. Natl Acad. Sci. USA*, **95**, 12123-12128.

Altschul, S. F., Madden, T. L., Schaffer, A. A., Zhang, J., Zhang, Z., Miller, W. & Lipman, D. J. (1997). Gapped BLAST and PSI-BLAST: a new generation of protein database search programs. *Nucl. Acids Res.* **25**, 3389-3402.

Aravind, L. & Koonin, E. V. (1999). Fold prediction and evolutionary analysis of the POZ domain: structural and evolutionary relationship with the potassium channel tetramerization domain. *J. Mol. Biol.* **285**, 1353-1361.

Aumailley, M., Mann, K., von der Mark, H. & Timpl, R. (1989). Cell attachment properties of collagen type VI and Arg-Gly-Asp dependent binding to its α2(VI) and α3(VI) chains. *Exp. Cell Res.* **181**, 463-474.

Chicheportiche, A. & Vasalli, P. (1994). Cloning and expression of a mouse macrophage cDNA coding for a membrane glycoprotein of the scavenger receptor cysteine-rich domain family. *J. Biol. Chem.* **269**, 5512-5517.

Engel, J. (1994). Electron microscopy of extracellular matrix components. *Methods Enzymol.* **245**, 469-488.

Freeman, M., Ashkenas, J., Rees, D. J. G., Kingsley, D. M., Copeland, N. G., Jenkins, N. A. & Krieger,

M. (1990). An ancient, highly conserved family of cysteine-rich protein domains revealed by cloning type I and type II murine macrophage scavenger receptors. *Proc. Natl Acad. Sci. USA,* **87**, 8810-8814.

Friedman, J., Trahey, M. & Weissman, I. (1993). Cloning and characterization of cyclophilin C-associated protein: a candidate natural cellular ligand for cyclophilin C. *Proc. Natl Acad. Sci. USA,* **90**, 6815-6819.

Fukami, A. & Adachi, K. (1965). A new method of preparation of a self-perforated micro plastic grid and its application (I). *J. Electron Microsc.* **14**, 112-118.

Hohenester, E., Sasaki, T. & Timpl, R. (1999). Crystal structure of a scavanger receptor cysteine-rich domain sheds light on an ancient superfamily. *Nature Struct. Biol.* **3**, 228-232.

Iacobelli, S., Arno, E., D'Orazio, A. & Coletti, G. (1986). Detection of antigens recognized by a novel monoclonal antibody in tissue and serum from patients with breast cancer. *Cancer Res.* **46**, 3005-3010.

Iacobelli, S., Bucci, I., D'Egidio, M., Guiliani, C., Natoli, C., Tinari, N., Rubinstein, M. & Schlessinger, J. (1993). Purification and characterization of a 90 kDa protein released from human tumors and tumor cell lines. *FEBS Letters,* **319**, 59-65.

Inohara, H. & Raz, A. (1994). Identification of human melanoma cellular and secreted ligands for galectin-3. *Biochem. Biophys. Res. Commun.* **201**, 1366-1375.

Inohara, H., Akahani, S., Koths, K. & Raz, A. (1996). Interactions between galectin-3 and Mac-2-binding protein mediate cell-cell adhesion. *Cancer Res.* **56**, 4530-4534.

Kohfeldt, E., Maurer, P., Vannahme, C. & Timpl, R. (1997). Properties of the extracellular calcium binding module of the proteoglycan testican. *FEBS Letters,* **414**, 557-561.

Koths, K., Taylor, E., Halenbeck, R., Casipit, C. & Wang, A. (1993). Cloning and characterization of a human Mac-2 binding protein, a new member of the superfamily defined by the macrophage scavenger receptor cysteine-rich domain. *J. Biol. Chem.* **268**, 14245-14249.

Li, X., Lopez-Guisa, J. M., Ninan, N., Weiner, E., Rauscher, F. J., III & Marmorstein, R. (1997). Overexpression, purification, characterization, and crystallization of the BTB/POZ domain from the PLZF oncoprotein. *J. Biol. Chem.* **272**, 27324-27329.

Linsley, P. S., Horn, D., Marquardt, H., Brown, J. P., Hellstrom, I., Hellstrom, K.-E., Ochs, V. & Tolentino, E. (1986). Identification of novel serum protein secreted by lung carcinoma cells. *Biochemistry,* **25**, 2978-2986.

Müller, S. A., Goldie, K. N., Bürki, R., Häring, R. & Engel, A. (1992). Factors influencing the precision of quantitative scanning transmission electron microscopy. *Ultramicroscopy,* **46**, 317-334.

Natali, P. G., Wilson, P. S., Imai, K., Bigotti, A. & Ferrone, S. (1982). Tissue distribution molecular profile, and shedding of a cytoplasmic antigen identified by the monoclonal antibody 465. 125 to human melanoma cells. *Cancer Res.* **42**, 583-589.

Ochieg, J., Leite-Browning, M. L. & Warfield, P. (1998). Regulation of cellular adhesion to extracellular matrix proteins by galectin-3. *Biochem. Biophys. Res. Commun.* **246**, 788-791.

Pearson, A. M. (1996). Scavenger receptors in innate immunity. *Curr. Opin. Immunol.* **8**, 20-28.

Ralston, G. (1993). *Introduction to Analytical Ultracentrifugation*, Beckman Instruments, Fullerston, USA.

Resnik, D., Pearson, A. & Krieger, M. (1994). The SRCR superfamily: a family reminiscent of the Ig superfamily. *Trends. Biochem. Sci.* **19**, 5-8.

Robinson, D. N. & Cooley, L. (1997). *Drosophila* kelch is an oligomeric ring canal actin organizer. *J. Cell Biol.* **138**, 799-810.

Rosenberg, I., Cherayil, B. J., Isselbacher, K. J. & Pillai, S. (1991). Mac-2-binding glycoproteins. Putative ligands for cytosolic α-galactoside lectin. *J. Biol. Chem.* **266**, 18731-18736.

Sasaki, T., Brakebusch, C., Engel, J. & Timpl, R. (1998). Mac-2 binding protein is a cell-adhesive protein of the extracellular matrix which self-assembles into ring-like structures and binds β1 integrins, collagens and fibronectin. *EMBO J.* **17**, 1606-1613.

Sato, S. & Hughes, R. C. (1992). Binding specificity of a baby hamster kidney lectin for H type I and II chains, polylactosamine glycans, and appropriately glycosylated forms of laminin and fibronectin. *J. Biol. Chem.* **267**, 6983-6990.

Seetharaman, J., Kanigsberg, A., Slaaby, R., Leffler, H., Barondes, S. H. & Rini, J. M. (1998). X-ray crystal structure of the human galectin-3 carbohydrate recognition domain at 2.1-Å resolution. *J. Biol. Chem.* **273**, 13047-13052.

Stock, D., Nederlof, P. M., Seemuller, E., Baumeister, W., Huber, R. & Lowe, J. (1996). Proteosome: from structure to function. *Curr. Opin. Biotechnol.* **7**, 376-385.

Trahey, M. & Weissman, I. L. (1999). Cyclophilin C-associated protein: a normal secreted glycoprotein that down-modulates endotoxin and proinflammatory responces *in vivo*. *Proc. Natl Acad. Sci. USA,* **96**, 3006-3011.

Ullrich, A., Surest, I., D'Egidio, M., Jallal, B., Powell, T. J., Herbst, R., Dreps, A., Azam, M., Rubinstein, M., Natoli, C., Shawver, L. K., Schlessinger, J. & Iacobelli, S. (1994). The secreted tumor associated antigen 90 K is a potent immune stimulator. *J. Biol. Chem.* **269**, 18401-18407.

Woo, H. J., Lotz, M. M., Jung, J. U. & Mercurio, A. M. (1991). Carbohydrate-binding protein 35 (Mac-2), a laminin binding lectin, forms functional dimers using cysteine 186. *J. Biol. Chem.* **266**, 18419-18422.

Yang, R. Y., Hill, P. N., Hsu, D. K. & Liu, F. T. (1998). Role of the carboxyl-terminal lectin domain in self-association of galectin-3. *Biochemistry,* **37**, 4086-4092.

Edited by R. Huber

(Received 12 April 1999; received in revised form 27 June 1999; accepted 27 June 1999)